Permeability of Small Molecules through a Lipid Bilayer: A Multiscale Simulation Study

Mario Orsi,[†] Wendy E. Sanderson,[‡] and Jonathan W. Essex*,[†]

School of Chemistry, University of Southampton, Southampton, SO17 1BJ United Kingdom, and Johnson & Johnson PRD, Janssen Pharmaceutica NV, Beerse, 2340 Belgium

Received: April 8, 2009; Revised Manuscript Received: June 25, 2009

The transmembrane permeation of eight small (molecular weight <100) organic molecules across a phospholipid bilayer is investigated by multiscale molecular dynamics simulation. The bilayer and hydrating water are represented by simplified, efficient coarse-grain models, whereas the permeating molecules are described by a standard atomic-level force-field. Permeability properties are obtained through a refined version of the *z*-constraint algorithm. By constraining each permeant at selected depths inside the bilayer, we have sampled free energy differences and diffusion coefficients across the membrane. These data have been combined, according to the inhomogeneous solubility−diffusion model, to yield the permeability coefficients. The results are generally consistent with previous atomic-level calculations and available experimental data. Computationally, our multiscale approach proves 2 orders of magnitude faster than traditional atomic-level methods.

Introduction and Background

Transport phenomena across biomembranes are fundamental processes in cellular biology. They are also becoming increasingly important in many medical, pharmaceutical, and environmental technologies.[1] For example, drug permeation is crucial to bioavailability, and is at the basis of the technology of liposomal transport systems.[2] Although important permeation mechanisms, such as those responsible for the translocation of sugars and amino acids, are actively controlled by proteins, *passive* permeation is the most common way by which solutes cross cell membranes. Most small molecules (such as water) and drugs are passively transported. While experiment can measure permeability coefficients, the exact mechanism of unassisted transmembrane transport is still not fully understood, as local membrane−solute interactions are difficult to probe. In fact, the current understanding of membrane permeability is still influenced by the theories developed over a century ago by Overton, who proposed that the membrane permeability coefficient of a solute can be simply correlated to its oil/water partition coefficient.[3] This observation led to the crude representation of the membrane as a homogeneous oil slab; on this basis, the simple bulk solubility−diffusion model of membrane permeability was proposed.[4] In more recent years, experiments have clearly established that lipid membranes are highly heterogeneous systems, very different from uniform oil phases; for instance, density distributions, order parameters, and diffusion in lipid membranes show characteristic properties that are not present in bulk oil systems. Moreover, lipid bilayers comprise highly polar moieties, such as the headgroup and the glycerol/ester regions, that do not have any counterpart in oil solvents. The heterogeneity present inside membranes is included in the *inhomogeneous* solubility−diffusion model,[5−7] which relates the permeability coefficient to the variations of local properties across the membrane; these properties, such as partitioning and diffusion of a solute as a function of its position inside the membrane, are extremely difficult to measure experimentally.

Particle-based simulations can provide insights into the understanding of transport phenomena across bilayers with the necessary resolution. In recent years, standard atomic-level (AL) molecular dynamics simulations have indeed been successfully employed to predict permeability coefficients and to investigate the general mechanism of passive transport across membranes.[2,8,9] These investigations have been extremely useful in understanding many aspects of bilayer permeation with atomic resolution. However, the huge computational cost of simulating AL membrane models causes a number of problems. For example, obtaining well-converged data can be difficult, as series of long simulations are required for every solute. Also, bilayer sizes must be rather small to be computationally amenable; this can induce artifacts, especially when large drugs are inserted into the membrane. Furthermore, the number of different permeants that can be investigated in a reasonable amount of time is extremely limited; this seriously hinders potential applications in the context of drug design, where the screening of large sets of candidate compounds is normally required. It is therefore highly desirable to develop techniques that can improve the efficiency of simulation.

A possible way to alleviate the AL computational cost involves simplifying the representation of the system via coarse-grain (CG) techniques. CG approaches generally involve grouping together entire clusters of atoms into single macro-sites, to significantly reduce the number of interactions calculated, and hence also the computational cost. CG methods can increase simulation speed by several orders of magnitude with respect to corresponding AL methods, while still retaining the most important physical features of the systems and phenomena represented.[10−12] However, membrane permeability is known to be extremely sensitive to the chemical identity of the permeating species; minor variations in the solute atomic structures can lead to differences of many orders of magnitude in the permeability coefficients.[13] In the context of transmembrane permeability, standard CG models are therefore unlikely to provide accurate descriptions. A natural compromise would involve combining the accuracy of AL force-fields to the

* To whom correspondence should be addressed. Tel.: +44 (0)23 8059 2794. Fax: +44 (0)23 8059 3781. E-mail: j.w.essex@soton.ac.uk.
[†] University of Southampton.
[‡] Johnson & Johnson PRD.

10.1021/jp903248s CCC: $40.75
Published on Web 08/10/2009

efficiency of CG models in a multiscale fashion.[14−16] This can be done by multiresolution models,[14] also called concurrent schemes,[16] where the "chemically sensitive" parts of the system (for example, the solutes in membrane permeation studies) are modeled atomistically, while the surrounding environment is simplified with CG representations. It would be particularly advantageous for such multiscale methods to be compatible with standard AL force-fields, which have been developed, tested, and successfully used for decades now. Several multiresolution approaches have been reported in the literature.[17−24] While these methods are generally promising, a number of issues can be noted. Most of the multiresolution schemes developed so far are characterized by the use of rather complex algorithms to specifically model the interfacial region between the AL and CG parts of the system. None of these techniques has been used to simulate transmembrane permeation processes. In fact, applications to biological systems have been so far limited to the modeling of basic structural and dynamical properties of proteins,[18,19] and to the study of the structure of a preassembled membrane−protein system.[20] In these approaches, problems arise whenever molecules diffuse across regions of different representations, as the models for the AL and CG particles are not compatible. Adaptive techniques, which address this issue by allowing changes of resolution across a predefined interface between the AL and CG regions, have been proposed only recently, and thus far have been applied to rather simple systems, such as idealized tetrahedral solvent particles,[22] liquid methane,[17,21] water,[24] and a generic solvated bead−spring polymer.[23] General problems involve the preservation of realistic dynamics and the consistency of relative dynamics across the different representation levels.[14]

In this study, we present multiscale simulations based on a simple and direct AL−CG coupling, where the different representations interact through compatible potentials. In particular, AL models of solute molecules are embedded in a bilayer represented at the CG level; mixed AL−CG interactions are treated "naturally" using standard mixing rules, without the need to carry out extensive parametrizations or to define interface regions. Such a straightforward multiresolution coupling is possible thanks to the characteristics of our CG membrane model,[25] which retains compatibility with AL force-fields, particularly with respect to the electrostatics. We have recently presented a proof of principle for the validity of our multiscale methodology by calculating water−octane partition coefficients for a set of AL amino acid side chains embedded into CG solvent representations.[26] In the study presented here, we extend and apply this multiscale approach to molecular dynamics simulation of the permeability of small AL solutes in a CG lipid membrane. In the next section, the models we employ, as well as the multiscale strategy, are summarized. Moreover, we present the theory underlying our permeability calculations. Data obtained from the multiscale permeability simulations are then presented and compared to standard AL simulation results and available experimental data. We then discuss our findings, along with advantages, limitations, and issues of our multiscale methodology. Ongoing work and future possible extensions are also mentioned.

Simulation Methodology

Coarse-Grain Models of Membrane and Water. The simulated bilayer membrane is represented by our recently developed CG model for dimyristoylphosphatidylcholine (DMPC) lipid bilayers.[25] In this simplified model, each lipid molecule, in reality comprising more than one hundred atoms, is reduced to ten macrounits. The lipid headgroup is coarse-grained into two Lennard-Jones spherical units, describing the choline and phosphate moieties. Headgroup electrostatics are represented by a positive point-charge embedded in the choline group and a negative one in the phosphate group. The glycerol and hydrocarbon regions are modeled by soft uniaxial ellipsoids through the Gay−Berne potential.[27] The Gay−Berne potential can be seen as an extension of the (isotropic) Lennard-Jones potential, where extra terms are added to allow the modeling of nonspherical (anisotropic) particles. In particular, the glycerol-ester region is described by two Gay−Berne ellipsoidal units, each embedded with a point-dipole to capture the dipolar charge distribution in this region. Hydrocarbon tails are modeled by chains of three neutral Gay−Berne ellipsoids; each ellipsoid represents a segment of four consecutive methyl groups. Intralipid bonds are modeled by the Hooke (harmonic) potential, as is standard practice. No angle or torsional potentials are present. Some of the force-field parameters have been recently refined; the new parameter set, employed in the simulations reported in this article, is described and tabulated in the Supporting Information. A manuscript detailing the results obtained with this new force-field, as well as its extension to different lipid species, is in preparation.

Water molecules are represented by the soft sticky dipole (SSD) model,[28] with parameters optimized for electrostatic cutoff simulations.[29] The SSD water is a single-site model; the three atoms of individual water molecules are coarse-grained into a single interaction center, which comprises a Lennard-Jones core providing excluded-volume, a point-dipole to model electrostatics, and a tetrahedral "sticky" term to capture hydrogen bonding. Detailed formulas of the SSD potential, and corresponding forces and torques, can be found elsewhere.[30] The SSD model is computationally much cheaper than the traditional AL multisite water models,[31,32] yet it accurately reproduces structural, thermodynamic, dielectric, dynamic, and temperature-dependent properties of real water.[28−30,33]

Atomic-Level Models of Small Molecules. We have selected the following solute candidates, representing common chemical functional groups: acetamide, acetic acid, benzene, ethane, methanol, methylacetate, methylamine, and water. We have chosen this set of molecules because it will enable comparison with the results obtained in a corresponding investigation carried out by standard AL methods.[34] Water is modeled by the SSD potential,[28,29] as described in the previous section. The other solutes are described by all-atom models. The atomic-level structures were produced with the program Molden.[35] The *antechamber* tool from the AMBER program[36] was then used to optimize the geometry, assign the Lennard-Jones parameters from the GAFF force-field,[37] and generate partial charges with the AM1/BCC model.[38] The solute models have no net charge; this is consistent with the assumption that only the neutral species diffuse across the bilayer.[39] For simplicity, no intramolecular degrees of freedom are taken into account, that is, solute molecules are rigid. All solutes are small, relatively compact molecules; it seems therefore reasonable to model them as rigid bodies.

To optimize the stability of molecular dynamics numerical integration, the atomic masses of some (typically, the lighter) permeants, that is, ethane, methanol, methylacetate, and methylamine, were redistributed. For these solutes, the mass of the hydrogen atoms was increased, while reducing accordingly the mass of the other atom types to roughly maintain the original total molecule mass. Since hydrogens are normally located on the periphery of molecules, this mass redistribution increases

the principal moments of inertia. This stabilizes the rotational motion, potentially allowing larger integration time steps to be used.[40] In fact, the procedure described has enabled us to maintain the large integration time step (20 fs) employed for the purely coarse-grain simulations,[25] thus preserving the efficiency of the method. Thermodynamic properties and center of mass dynamics are not affected by such an alteration of the principal moments of inertia, while rotational dynamics are expected to slow down. Since the permeability coefficient depends on the (linear) diffusion coefficient of the molecular center of mass (see also the following eq 3), our permeability calculations for these molecules will not be affected by the mass redistribution. The SSD water model implemented represents a special case, as the total mass has been substantially increased, from 18 to 50 amu. However, in a previous test[25] we observed that the linear diffusion coefficient decreased by only 20%. Hence, even in the case of our "heavy" SSD water model we predict negligible effects on the overall permeability properties. The remaining solutes (acetic acid, acetamide, benzene), naturally characterized by sufficiently large principal moments of inertia, did not present integration stability problems and hence were assigned normal atomic masses. The specific values of atomic masses and principal moments of inertia for all molecules are reported in the Supporting Information.

Mixed AL−CG Interactions. All the potentials employed to represent the various interacting sites in our multiresolution membrane−water−solute systems are directly compatible with each other. Therefore, mixed interactions between CG sites and AL atoms can be treated straightforwardly by available formulas. In particular, Lennard-Jones cross terms between lipid headgroups, water, and solute atoms are calculated using standard mixing rules.[41] Mixed Lennard-Jones/Gay−Berne interactions are consistently treated using the generalized Gay−Berne potential,[42] which accounts for the intralipid headgroup−tail interactions, the interaction between the Lennard-Jones term of the SSD potential and the Gay−Berne lipid term, and the interaction between the Lennard-Jones terms of the AL solutes and the Gay−Berne lipid term. Explicit formulas of potentials, forces, and torques for both the original Gay−Berne model and its generalized version are reported in detail elsewhere.[27,42,43] In our model we represent explicitly all relevant electrostatics of the lipid, water, and solute molecules through point charges (monopoles) and point dipoles, as described previously. Therefore, monopole−monopole, monopole−dipole and dipole−dipole interactions can be simply described by standard electrostatic formulas.[44] Despite being able to directly treat the mixed AL−CG interactions, some ad hoc adjustments should be expected, given that we are mixing two rather different empirical models, that is, our coarse-grain force-field and the GAFF atomic-level force-field.[37] In fact, preliminary work to calibrate the mixed parameters between CG and AL sites was previously carried out by calculations of water−octane partition coefficients for a range of solutes by Monte Carlo simulations.[26] Octane molecules were modeled as pairs of Gay−Berne ellipsoids connected by a harmonic spring, using the parameters developed for the hydrocarbon tails of our CG lipid model,[25] water was represented with the SSD potential,[28,29] and the solutes with the GAFF all-atom force-field.[37] The solutes used were 15 analogues of neutral amino acid side chains. In that work,[26] results could be brought into excellent agreement with experimental data by introducing two scaling factors into the standard mixing rules, to modify the electrostatic potential energy term between water and solutes, and the generalized Gay−Berne potential energy term between lipid tail sites and solutes. That study[26] proved that a general, transferable multiscale model for our CG model and a standard AL force-field can be obtained through a fast and simple calibration involving only two extra parameters. In fact, the scaling factor α controlling the electrostatic interaction between CG water and AL solutes has been transferred unaltered to the simulations reported in this article. In particular, the electrostatic energy U_{ij}^{E} between an AL atom i, bearing the partial charge Q_i, and an SSD water site j, characterized by the dipole μ_j, is calculated as

$$U_{ij}^{E} = \alpha \frac{Q_i \boldsymbol{\mu}_j \mathbf{r}_{ij}}{4\pi\varepsilon_0 |\mathbf{r}_{ij}|^3} \quad (1)$$

where α is the additional scaling factor, ε_0 is the permittivity of vacuum, and $\mathbf{r}_{ij}$ the distance between the interacting pair. Following our previous calibration work,[26] we therefore set $\alpha = 1.1$. The second scaling factor controls the Lennard-Jones/Gay−Berne mixed energy term ε_{ij} between an AL atom i and an ellipsoidal CG site j:

$$\varepsilon_{ij} = \beta\sqrt{\varepsilon_i \varepsilon_j} \quad (2)$$

where β is the additional scaling factor, ε_i is the Lennard-Jones energy term for atom i, and ε_j is the Gay−Berne energy term for the coarse-grain site j. In our previous multiscale calculation of solvation free energies for AL solutes in CG octane[26] it was observed that, without scaling the mixed interaction term ε_{ij} (that is, setting $\beta = 1$), the solutes would favor too much the CG apolar phase, resulting in an overestimation of partition coefficients. This was fixed by simply reducing β; in particular, the target data were fitted by setting $\beta = 0.8$. To a first approximation, it would be tempting to directly transfer this value for β to the systems investigated in this article. However, we are here considering an interfacial membrane system, rather different from the homogeneous bulk-phase octane system employed in the previous multiscale study,[26] and hence such a transfer may not be physically justified. We therefore decided to specifically parametrize β for solute−lipid interactions; this could be done in a fast and simple way, using a similar approach to that employed in our previous multiscale investigation.[26] In particular, we select as parametrization targets the permeability coefficient data obtained from AL simulations of a set of small organic molecules.[34] Using the methodology described in the next section, preliminary multiscale permeability simulations were carried out to identify the value for β that could best fit the target data. As observed for the octane study,[26] simply leaving $\beta = 1$ revealed a tendency of the multiscale model to overestimate the partitioning of the AL solutes into the CG apolar region, in this case corresponding to the lipid hydrocarbon core of the membrane. This initially led to transmembrane permeability coefficients larger than those obtained in the reference AL investigation.[34] To calibrate the mixed interactions, β was decreased until the target data could be reproduced; in this case, the best fit was obtained for $\beta = 0.5$. This value for β has therefore been adopted for the simulations presented in the reminder of the article. It will be seen that the fitting of this single parameter allows accurate permeability predictions for all the eight solutes selected, both in terms of absolute magnitudes and regarding the relative rankings; this is not trivial, given that the solutes are rather diverse and characterized by permeability coefficients spanning several orders of magnitude.

The Inhomogeneous Solubility−Diffusion Model. The inhomogeneous solubility−diffusion model[5−7] relates the (experimentally measurable) permeability coefficient of a solute to an integral of depth-dependent parameters across the membrane. In particular, the transmembrane permeability coefficient P is expressed as

$$P = 1/\int_{z_1}^{z_2} R(z)\,\mathrm{d}z = 1/\int_{z_1}^{z_2} \frac{\exp(\Delta G(z)/k_B T)}{D_z(z)}\,\mathrm{d}z \quad (3)$$

where $R(z)$, $\Delta G(z)$, and $D_z(z)$ are the solute resistance, the transfer free energy, and the z component of the diffusion coefficients, respectively, at position z along the direction normal to the membrane interfacial plane. Precisely, the transfer free energy $\Delta G(z)$ represents the difference between the free energy at position z across the bilayer and the reference value in the water phase, which we assume to be zero. The integration extremes z_1 and z_2 are taken in the water phases at the two sides of the membrane, so that the integration is performed over the entire bilayer. The quantities featuring in the inhomogeneous solubility−diffusion model (eq 3) can be obtained from simulation by applying the z-constraint method.[7,45−47] For this work, we have developed an alternative implementation of the z-constraint method which guarantees the conservation of all relevant physical quantities; the algorithm is detailed in the Supporting Information.

Permeability Simulation Protocol. Molecular dynamics is carried out with our software BRAHMS.[25,48] The equations of motion are integrated using an advanced symplectic and time-reversible method,[49] with a time step of 20 fs. Pressure and temperature are maintained at 1 atm and 30 °C using the weak-coupling scheme.[50] Lipid, water, and solute temperatures are coupled separately with time constants $\tau_T = 0.1$ ps for lipid and water, and $\tau_T = 0.02$ ps for the solute. The pressure is controlled by semi-isotropic volume scaling with time constant $\tau_P = 0.2$ ps and isothermal compressibility $\beta = 4.6 \times 10^{-5}$ atm^{-1}. The cutoff radius for both Lennard-Jones and electrostatic water−water interactions is 0.9 nm, as prescribed for the SSD parametrization adopted.[29] All other nonbonded cutoff radii have been set to 1.2 nm. Electrostatic interactions are treated using cutoff schemes. In particular, all charge−charge and charge−dipole interactions (including those between AL and CG sites) are implemented using the shifted-force cutoff method.[41] We employ the SSD parameters optimized to evaluate dipole−dipole interactions with a cubic switching cutoff scheme;[29] for consistency, all dipole−dipole interactions are treated in this manner. Nonbonded interactions involving solute molecules are treated as group-based with a cutoff distance of 1.2 nm; the interactions between all solute atoms and the interacting site (either a lipid or a water site) are evaluated if the distance between the solute mass center and the interacting site is less than the cutoff. The bilayer model employed is a CG membrane comprising 128 DMPC lipids and 3400 hydrating SSD water molecules.[25] For each of the AL solutes, the z-constraint method has been applied to sample 16 equally spaced z-positions across one monolayer; results are considered valid also for the other monolayer by symmetry. In particular, we have sampled distances from 3.1 to 0.1 nm from the bilayer center in 0.2 nm increments along the z-axis (normal to the membrane plane). In each simulation, a single solute molecule was present in the bilayer. For each solute, 16 systems were prepared (to cover the selected z-depths). Molecules were initially inserted at 0.002% of their actual size, and with charges and Lennard-Jones parameters set to 0.002% of their actual values. The solutes were then incrementally grown back, and the interaction parameters incrementally increased toward their real values, over 50000 molecular dynamics steps, corresponding to 1 ns of simulation time. This insertion procedure proves robust, as it allows a gradual relaxation of the bilayer around the permeant. For each solute, the 16 systems were subsequently equilibrated for 10 ns. For each of these systems, production runs were then conducted for 80 ns, divided into two consecutive 40 ns batches. The simulation length was set to ensure convergence of the average constraint force, from which the solubility−diffusion parameters are derived (eq 3). A typical example of the time evolution of the constraint force on a solute during one of the permeability simulations is shown in Figure 1. It can be seen that the constraint force fluctuates significantly over time scales of a few tens of ns; our choice for a sampling time of 80 ns seems therefore appropriate. Using standard 2-GHz AMD Opteron processors, each 80 ns production run took just five days of CPU-time. All simulations could be run almost concurrently on the Iridis cluster[51] at the University of Southampton in a coarsely parallel fashion, meaning that each (independent) simulation ran on a different CPU. The entire set of simulations, totaling over 10 μs of simulation time, ran in about one week.

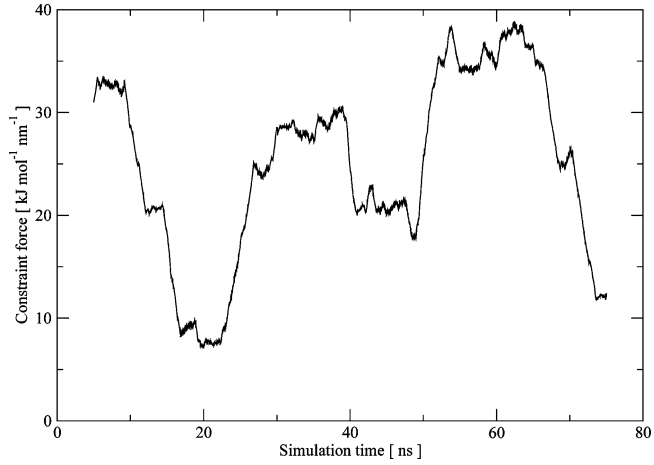

Figure 1. Constraint force on a molecule of acetic acid constrained at a distance of 0.1 nm from the bilayer center. For clarity, the data are represented as moving averages over 10 ns time windows; the plotted constraint force at x ns thus corresponds to the average over the time interval from $(x - 5)$ ns to $(x + 5)$ ns.

Results

In this section, we report the results obtained from the multiscale AL−CG permeability simulations. For the free energy, diffusion and resistance profiles, and for the overall permeability coefficients, we will report average values and standard errors computed from the averages over the two 40 ns consecutive blocks of each of the 80 ns runs. The data obtained will be compared to previous AL simulation studies and available experimental data. The CG membrane is a model for DMPC bilayers, and hence comparisons should ideally be made with results obtained with this lipid species. In fact, some experimental and simulation data for DMPC will be reported. However, we will consider many results obtained for dipalmitoylphosphatidylcholine (DPPC) lipid bilayers, as this was the lipid species employed in the AL investigation which constitutes our primary comparison source.[34] DPPC is structurally identical to DMPC apart from slightly longer tails (two more carbons).

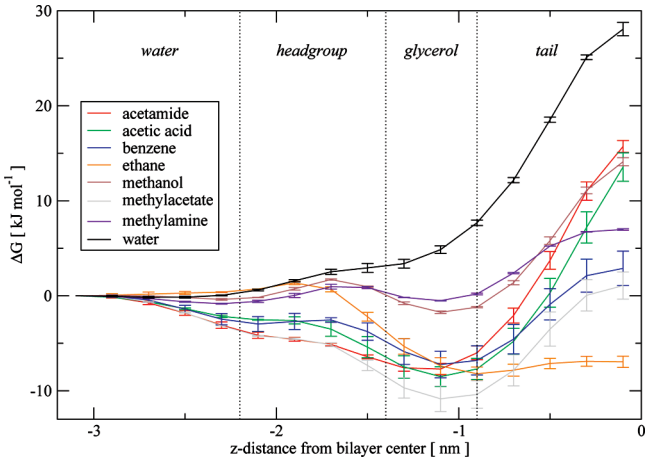

Figure 2. Free energies of transfer from water to selected z-positions along the bilayer normal. To facilitate interpretation, different regions across the system are marked in italics, namely, the bulk *water* region, the lipid *headgroup* region, the lipid *glycerol* region, and the hydrocarbon *tail* core. Approximate boundaries between these regions are defined by the vertical dotted lines.

Also, all data considered here refer to fully hydrated bilayers in the liquid-crystalline phase. Under these conditions, DPPC bilayers are only 0.2 nm thicker than DMPC bilayers;[52] this amounts to just ≈5% of the overall membrane thickness. Permeability properties are unlikely to be significantly affected by this difference, particularly in terms of *relative* permeabilities, which are our main focus. Therefore, we believe it is reasonable to compare results for DMPC to corresponding data for DPPC. We will also report a few experimental permeability coefficients derived from studies on lecithin bilayers, which are mixtures of different phosphatidylcholine (PC) lipids.

Free Energies of Transfer. For each of the solutes considered, the free energies of transfer from the water phase to the selected z-positions inside the membrane are reported in Figure 2. Considering the first part of the curves, from the water phase to the headgroup region, we can identify two types of behavior. The solutes ethane, methanol, methylamine, and water exhibit an overall slight free energy increase on entering the headgroup region. This behavior indicates a minor permeability-barrier effect in this region. The remaining half of the solutes (acetamide, acetic acid, benzene, methylacetate) show instead, in the same region, a free energy decrease; this corresponds to these permeants favoring the headgroup region with respect to the water phase.

Proceeding deeper into the bilayer, corresponding to the glycerol region, all molecules except water display a free energy decrease. In particular, most permeants (acetamide, acetic acid, benzene, ethane, and methylacetate) are characterized in this region by deep free energy minima, between −6 and −11 kJ/mol; these solutes are therefore predicted to preferably partition in this region. Methanol and methylamine display shallower local free energy minima, whereas the free energy of water continues monotonically to increase.

The rightmost part of the diagram in Figure 2 shows the change in free energy characterizing the solutes when constrained in the hydrocarbon tail region (the bilayer core). Here all solutes display a free energy increase, highlighting a barrier effect of the hydrocarbon tail region. A particularly steep free energy increase can be noticed for acetamide, acetic acid, benzene, methanol, methylacetate, and water. The free energy rise in this region is instead rather small for methylamine, and almost negligible for ethane.

A close comparison between the AL−CG free energy profiles and the corresponding curves calculated in the reference AL study[34] highlights a number of qualitative differences. In the lipid headgroup−glycerol region, all the AL profiles[34] display a free energy increase on entering the headgroup region. However, as already noted earlier, at the same location only half of the multiscale profiles are characterized by a free energy increase, whereas the remaining half display a shallow dip. Experimental data on the free energy difference between the headgroup region and the water phase have been obtained for acetic acid; from the partition coefficient in DMPC vesicles, a value $\Delta G \approx -0.45$ kJ/mol was calculated.[53] This negative value is in qualitative agreement with our AL−CG results, whereas it is inconsistent with the AL results, which gave a positive free energy difference.[34] However, there is a discrepancy of a factor of ∼5 between that experimental value[53] and our AL−CG result. Experiments have also been performed on short-chain alcohols including methanol. These data indicate that short-chain alcohols in general,[54−58] and methanol in particular,[54,55] preferentially locate inside the bilayer, and in particular in the polar/apolar interface region, comprising the headgroup, glycerol, and upper tail region. The AL−CG free energy curve for methanol displays a global minimum at $z = -1.1$ nm, thereby indicating a preferential partioning inside the membrane, in the glycerol and upper tail regions. Instead, the AL data by Bemporad et al.[34] do not show any free energy minimum inside the membrane, thus predicting a preferential location of methanol outside the bilayer, in the water phase. Patra et al.[59] also studied the interaction of methanol with lipid bilayers by AL simulation. In that study, 90 methanol molecules were inserted in the water phase of a membrane system comprising 128 lipids and ∼9000 water molecules. By calculating equilibrium density distributions, it was observed that methanol preferentially partitioned inside the bilayer, at an average distance of ∼1.4 nm from the bilayer center. This is consistent with our AL−CG prediction of a preferential location of methanol inside the bilayer, at ∼1.1 nm from the bilayer center. Patra et al.[59] also predicted the interaction of methanol with the membrane to be weak, as no penetration through the bilayer took place over the 50 ns simulation (by comparison, ethanol was instead found to permeate easily[59]). Such an observation is consistent with our AL−CG free energy curve for methanol, as the minimum is shallow (indicating weak association with the bilayer) and the central barrier is substantial (thus opposing penetration). Overall, the AL simulation results of Patra et al.[59] are therefore in line with the AL−CG data presented here. More evidence in support of our AL−CG results can be found in recent AL data[60,61] on the transfer free energies of the side chain analogues of the amino acids asparagine and serine, which are identical to acetamide and methanol, respectively. These free energy profiles[60,61] are consistent with our multiresolution results; in particular, negative global minima corresponding to the glycerol region can be identified for both molecules.

In general, in the glycerol region, all the AL−CG multiscale free energy profiles, except those for water and ethane, display minima at $z \approx -1.1$ nm, corresponding to a region that comprises the glycerol backbone and the upper tail methylene of the hydrocarbon region. In particular, acetamide, acetic acid, benzene, and methylacetate show in this location rather deep global free energy minima, of the order of −5 to −10 kJ/mol. For these molecules there are evident discrepancies with the corresponding AL data.[34] For example, the AL free energy curves for acetamide and acetic acid display global minima in the water phase outside the bilayer (for $z = -3$ nm), while

TABLE 1: Free Energy of Transfer of Water from the Outer Water Phase to the Bilayer Center[a]

multiscale (this work)	28.1 ± 0.7[c]
atomic-level[b]	22.9[34d] 22.5[63c] 26.0[7d] 26.4[62d] 56.5[64c]

[a] Values expressed in kJ/mol. [b] References are given. [c] Fluid-phase DMPC. [d] Fluid-phase DPPC.

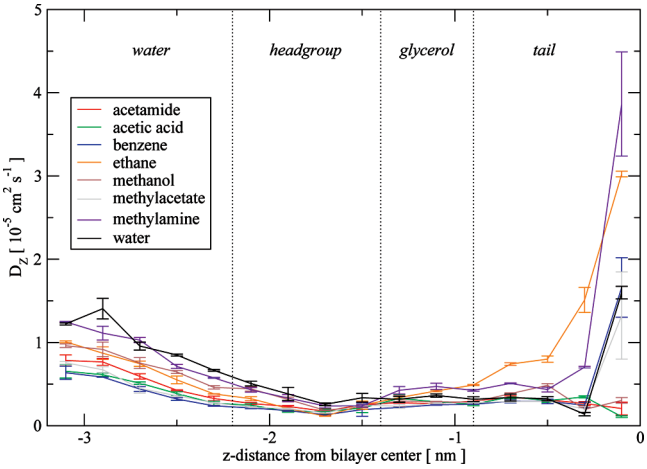

Figure 3. Diffusion coefficients along the z-dimension (normal to the membrane plane) for selected z-positions inside the bilayer. To facilitate interpretation, different regions across the system are marked in italics, namely, the bulk *water* region, the lipid *headgroup* region, the lipid *glycerol* region and the hydrocarbon *tail* core. Approximate boundaries between these regions are defined by the vertical dotted lines.

increasing monotonically across the glycerol region. The AL profile[34] for benzene does display a minimum inside the membrane, as in the multiscale data, whereas the AL curve[34] for methylacetate displays a very shallow minimum (as opposed to the deep minimum in the AL−CG result). The multiscale data for methylamine and methanol are characterized, in the glycerol region, by shallow minima, whereas the AL curves,[34] in the same region, monotonically increase. Ethane and water behave similarly for both the AL[34] and multiscale models in the glycerol region; ethane displays a minimum, whereas water is characterized by a clear free energy increase.

Deep inside the hydrocarbon tail core, most of the multiscale curves display a similar behavior to the AL results.[34] In particular, acetamide, acetic acid, methanol, methylamine, and water are characterized by overall increases. However, the data for benzene and methylacetate are not consistent; in the central hydrocarbon region, the free energy of these two solutes increases in the AL−CG results, whereas it remains constant in the AL data.[34]

Regarding the free energy of water, it is possible to compare our results to simulation data reported in the literature;[7,34,62−64] all these investigations yield curves qualitatively similar to that obtained from our simulations. The free energy values in the bilayer center, quantifying the water permeability barrier function of membranes, are collected in Table 1; it can be seen that our result lies inside the range of those obtained by AL methods.

Diffusion Coefficients. The diffusion profiles $D_z(z)$ are displayed in Figure 3. The values obtained with the AL−CG model are within 1 order of magnitude of the AL results reported in the simulation study of the same set of solutes.[34] However, qualitative discrepancies from that study[34] can be noted for a number of molecules. In particular, Figure 3 shows that the diffusion coefficients of benzene, ethane, methylamine, methylacetate, and water are higher in the center of the bilayer than in the outer water phase; these data do not agree with those

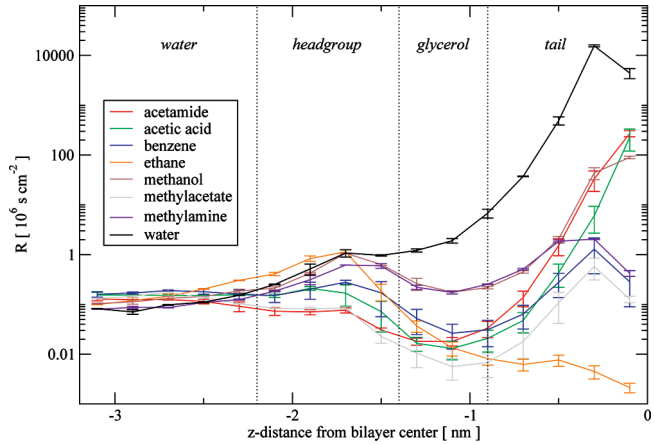

Figure 4. Resistance profiles. The curves connect resistance values calculated at selected z-positions along the bilayer normal. To facilitate interpretation, different regions across the system are marked in italics, namely, the bulk *water* region, the lipid *headgroup* region, the lipid *glycerol* region, and the hydrocarbon *tail* core. Approximate boundaries between these regions are defined by the vertical dotted lines.

reported in the AL simulation study[34] where, for all solutes, diffusion coefficients in the bilayer center were found to be significantly lower than in the water phase. However, two other previous AL investigations reported conflicting results. In the water permeability simulations by Marrink and Berendsen,[7] the diffusion rate in the bilayer center was reported to be more than twice as large as in the water phase. As noted elsewhere,[2] this discrepancy may stem from Marrink and Berendsen's modeling of the $-CH_2-$ and $-CH_3$ groups in the lipid tails without explicit hydrogens, that is, using a united-atom representation. However, Shinoda et al.,[62] using an explicit-hydrogen model, also reported the diffusion coefficient D_z for water in a DPPC bilayer to be twice as high in the hydrocarbon center than in the water phase. Moreover, in another molecular dynamics investigation of benzene in a DMPC bilayer with all hydrogens explicitly modeled, it was found that benzene diffused three times faster in the bilayer center than in the interfacial region;[65] in that case though, the total diffusion coefficient was calculated, as opposed to the z-component only (as considered in this study and the other referenced works). In all these studies,[7,62,65] the enhanced diffusion was ascribed to the small size of water and benzene; they diffuse faster by jumping between the free volume pockets available in the middle of the bilayer, which is in fact the lowest-density region of the system.

Resistances. Resistance profiles $R(z)$ as a function of the bilayer normal, calculated from $\Delta G(z)$ and $D_z(z)$ with eq 3, are displayed in Figure 4. It can be seen that the most hydrophilic solutes, which are acetamide, acetic acid, methanol, and water, are characterized by a net resistance increase from the water phase to the hydrocarbon core. Methylamine, benzene, and methylacetate display almost no overall change, whereas ethane shows a net resistance decrease. In general, the resistance profiles of Figure 4 show a clear correlation to the free energy profiles of Figure 2. This is expected, as in the solubility−diffusion model employed (eq 3) the resistance $R(z)$ depends largely on the free energy difference $\Delta G(z)$, which features as the argument of an exponential, while the contribution of the diffusion coefficient $D_z(z)$ is comparatively small. However, in some resistance profiles it is possible to identify slight deviations from the shape of the corresponding free energy profiles; these effects are determined by the diffusion coefficients (Figure 3). The local resistance is inversely proportional to the diffusion coefficient (eq 3); the observed enhanced diffusion of some solutes in the

TABLE 2: Permeability Coefficients[a]

		atomic-level		experiment	
solute	multiscale[b] (this work)	value	reference	value	reference
acetamide	$8.2 \pm 0.6 \times 10^{-2}$	$6.6 \pm 1.9 \times 10^{-3}$[c]	34	1.0×10^{-4}[d]	78
				1.7×10^{-4}[e]	70
				1.7×10^{-4}[e]	79
				2.9×10^{-4}[e]	39
				1.65×10^{-4}[e]	4
				4.5×10^{-4}[c]	80
acetic acid	$1.4 \pm 0.6 \times 10^{-1}$	$1.3 \pm 0.5 \times 10^{-1}$[c]	34	6.9×10^{-3}[e]	70
				6.6×10^{-3}[e]	81
				5.0×10^{-3}[e]	13
benzene	7.8 ± 2.6	10 ± 1[c]	34		
ethane	7.3 ± 0.6	6.7 ± 0.8[c]	34		
methanol	$1.8 \pm 0.2 \times 10^{-1}$	$1.9 \pm 0.4 \times 10^{-2}$[c]	34		
methylacetate	15.1 ± 2.3	9.5 ± 1.1[c]	34		
methylamine	3.3 ± 1.2	1.2 ± 0.2[c]	34	9×10^{-1}[e]	82
				8×10^{-2}[e]	70
water	$1.4 \pm 0.1 \times 10^{-3}$	6.8×10^{-2}[b]	63	8.3×10^{-3}[b]	83
		4.0×10^{-2}[c]	63	7.0×10^{-3}[b]	84
		$1.3 \pm 0.3 \times 10^{-2}$[c]	34	2.4×10^{-2}[b]	76
		1.6×10^{-2}[c]	62	4.0×10^{-4}[b]	77
		$7.0 \pm 3.0 \times 10^{-2}$[c]	7	1.0×10^{-3}[b]	77
				6.0×10^{-4}[b]	85
				2.4×10^{-3}[c]	86
				1.9×10^{-2}[c]	76
				1.5×10^{-2}[d]	78
				3.4×10^{-3}[e]	70
				2.2×10^{-3}[e]	4
				1.9×10^{-3}[e]	13

[a] Values in cm/s. References are included. [b] Fluid-phase DMPC. [c] Fluid-phase DPPC. [d] Fluid-phase DLPC. [e] Fluid-phase lecithin.

bilayer core should therefore affect resistances in that region. This effect can be observed for benzene, ethane, methylamine, methylacetate, and water, which display a resistance drop in the bilayer center despite the free energy increase observed in the same region (Figure 2); this resistance decrease is indeed determined by the increased diffusion of these solutes (discussed in the previous section).

Permeability Coefficients. The free energies of transfer $\Delta G(z)$ and diffusion data $D_z(z)$ have been combined according to the inhomogeneous solubility−diffusion model[5−7] (eq 3) to calculate the permeability coefficients. Table 2 reports the permeability coefficients computed for the eight solutes considered. Results obtained in this study, using a CG DMPC model mixed with AL solutes, are shown in the second column. The third column reports corresponding results obtained by standard AL simulations, whereas the fifth column shows available experimental data. The results obtained in this work are generally within 1 order of magnitude of the AL data, and within 2 orders of magnitude of the available experimental measurements. Since in our model we parametrized the AL−CG scaling factor β (defined in eq 2) to best fit the magnitude of the AL permeability coefficient data, this level of agreement is expected. However, it is most important to capture the solute *relative* permeability coefficients, which define the permeability ranking orders of the solutes, and these are generally independent from the extra parameter introduced. We observe that the permeability ranking orders obtained from the AL and the AL−CG multiscale methods are almost identical, as shown in Table 3. This result shows the high accuracy of the method in predicting a (crucial) property for which it was not directly fitted.

In the case of water, the permeability coefficient calculated here with the solubility−diffusion model parametrized via constraint simulations can be compared with that obtained by directly applying Fick's law on the observed spontaneous transmembrane flux of water molecules during long-time unconstrained molecular dynamics. By running our original CG model for 0.9 μs and counting the number of water molecules spontaneously crossing the membrane, we obtained a value of $9.2 \pm 0.4 \times 10^{-3}$ cm/s (details of the calculation can be found in the original reference[25]). We have also recently run a 1.2 μs unconstrained simulation with the refined force field used in the work presented here; the permeability coefficient obtained from that simulation was $5.1 \pm 0.6 \times 10^{-3}$ cm/s (unpublished result). These values are larger but of the same order of magnitude than that obtained here ($1.4 \pm 0.1 \times 10^{-3}$ cm/s). Considering the differences in the simulation methods (unconstrained vs constrained) and the permeation models (Fick vs solubility−diffusion) involved, this level of agreement is satisfactory.

TABLE 3: Comparison of Permeability Ranking Orders. Solutes are Listed in Order of Decreasing Permeability Coefficient

atomic-level (Bemporad et al.)[34]	multiscale (this work)
benzene	methylacetate
methylacetate	benzene
ethane	ethane
methylamine	methylamine
methanol	methanol
acetic acid	acetic acid
water	acetamide
acetamide	water

Solute Orientations, Membrane Perturbations, and Water Intrusions. By visually inspecting the trajectories, we notice that all solutes, when constrained in the outer water phase and in the lipid headgroup regions, are characterized by isotropic motion. Also, the presence of permeants in these regions does not influence the structure of the bilayer. However, when the permeants are constrained in the lipid glycerol and hydrocarbon

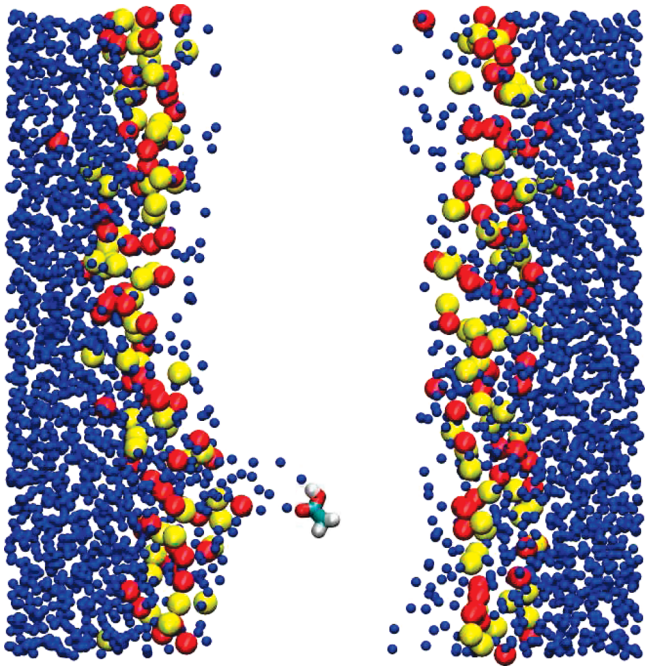

Figure 5. Simulation snapshot from a multiscale *z*-constraint simulation. The permeant acetic acid is constrained at 0.1 nm from the bilayer center toward the left monolayer. The CG choline, phosphate, and water sites are represented in red, yellow, and blue, respectively. The lipid tails are omitted for clarity. The AL solute acetic acid is colored by atom type, with hydrogen, oxygen and carbon colored gray, red, and green, respectively. Image prepared with VMD.[87]

regions, some interesting effects can be observed. The more polar solutes, that is, acetamide, acetic acid, and methanol, clearly show a tendency for preferential orientations. In particular, these molecules tend on average to point their oxygen atoms (their most polar moieties) away from the hydrocarbon center and toward the headgroup and water regions. Also, these solutes typically induce local perturbations, such as intrusions of water and headgroups into the hydrocarbon region. As an example, Figure 5 shows a snapshot from a simulation with acetic acid; the permeant induces the formation of a water "finger", and it locally attracts some lipid headgroups. Similar effects have been observed for acetic acid in a standard AL simulation by Bemporad et al.;[66] that study is also consistent with ours in showing that acetic acid orients its oxygens toward the water−lipid interface. Moreover, that AL simulation showed the formation of a water column local to the solute,[66] a membrane "defect" similar to that observed here (Figure 5). This behavior was also observed by Patra et al. in their simulation study involving methanol.[59] They noticed how methanol molecules move together with small clusters of water molecules when trying to enter the membrane.[59] Figure 6 shows two snapshots of our AL−CG multiscale simulations of methanol constrained at a distance of 0.1 nm from the bilayer center; the presence of water molecules closely interacting with the permeating methanol can be clearly seen. The rest of the solutes, that is, benzene, ethane, methylacetate, and methylamine, induce less pronounced local perturbations compared to those observed for the most polar molecules. In general, the effects observed can therefore be related to the degree of polarity of a permeant. When residing in the glycerol and hydrocarbon regions, highly polar (hydrophilic) solutes attract hydrating water and interact with headgroups, whereas nonpolar (hydrophobic) solutes do not significantly perturb the bilayer.

Discussion

We have presented a new multiscale AL−CG model where the two levels of resolution (atomic-level and coarse-grain) interact without the need for an interface. This is possible thanks to the unique nature of our CG model,[25] which consists of potentials directly compatible with AL force-fields. In particular, both lipid and water CG models contain all relevant electrostatics; this feature, which is not present in any other CG model, allows the AL−CG electrostatic interactions to be treated straightforwardly. By adopting a CG description of the membrane, we could increase the simulation efficiency to explore larger systems for longer times than has been done with standard AL simulations. We studied the interaction of solutes with a bilayer system comprising 128 lipids, larger than the typical 36−72 lipid bilayers that have been simulated by standard AL methods in permeability calculations.[7,34,45,62−64,67,68] Large membranes minimize artifacts from periodicity (due to the periodic boundary condition normally assumed in molecular dynamics) and are less likely to suffer from structural distortions caused by the permeant inclusions (this problem being particularly serious when large solutes, such as drugs, are considered). For each solute, we have sampled selected depths across the membrane for 80 ns, a much longer time than that (<10 ns) typically reached in corresponding AL permeability simulations.[7,34,45,62,63,68] Each 80 ns run, often necessary to reach convergence, took only five days of CPU-time on a standard computational processor. By comparing the simulation cost of our multiresolution model to corresponding AL calculations,[34] a speed-up factor of 2 orders of magnitude can been estimated. We could run all simulations reported in this article almost simultaneously on a cluster;[51] a total of over 10 μs of simulation data were produced in about one week.

The permeability results obtained by the AL−CG method were generally within 1 order of magnitude of those obtained in a reference AL study[34] and within 2 orders of magnitude of available experimental data (Table 2); more importantly, the relative permeabilities, and hence also the ranking order, are in good agreement (Table 3). Results indicate that the overall permeability is mainly determined by the free energy component, the diffusion contribution being rather marginal; such findings agree with previous analysis.[34,69]

Regarding the diffusion profiles, we have already pointed out that in the AL−CG profiles (Figure 3) most solutes display diffusion coefficients in the center of the bilayer which are higher than in the water phase, whereas in the AL simulations[34] the diffusion coefficients for all solutes were found to be significantly lower inside the bilayer than in the water phase. We also noticed that there are literature data more in line with the AL−CG results, at least for water[7,62] and benzene.[65] Also, experimentally, solutes with low molecular weight (<50) have been found to permeate significantly faster than predicted by Overton's theory.[70] This discrepancy has been explained with the free-volume model, according to which small-sized solutes diffuse abnormally fast by jumping between mobile free-volume pockets which are too small to accommodate larger solutes.[71] Free-volume voids form dynamically by lateral density fluctuations in the lipid hydrocarbon region of membranes.[72] As noted elsewhere,[2] this hypothesis is also supported by simulation data on large (molecular weight $\approx$ 300) solutes, for which the diffusion coefficient is almost independent of the depth inside the bilayer;[66,71,73] this can be rationalized considering that those permeants are too large to jump through the free-volume pockets. It could be argued whether CG membrane models can adequately capture free-volume effects. Our specific model has

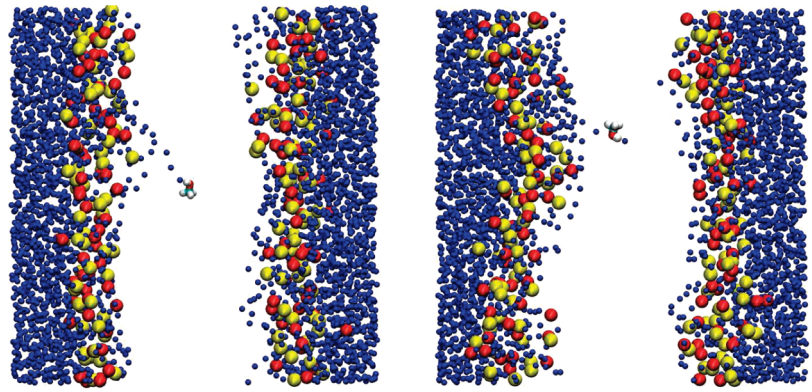

Figure 6. Simulation snapshots from a multiscale simulation with the permeant methanol constrained at 0.1 nm from the bilayer center toward the left monolayer. The color code is described in the legend of Figure 5.

proved consistent in this respect; the experimental lipid lateral diffusion coefficient was accurately reproduced, and mass-center traces were shown to be consistent with the free-volume model.[25]

In general, several possible reasons can account for the discrepancies observed between the AL−CG results presented here and the corresponding AL data.[34] First, there are significant differences in the models. The AL model[34] explicitly represents every atom, whereas, in the AL−CG system, the bilayer representation is substantially simplified.[25] The solutes, in particular, are modeled atomistically in both studies, but with different force-fields, that is, CHARMM[74] for the AL model[34] and GAFF[37] for our AL−CG model. Second, simulation conditions are also somewhat different. The AL−CG simulations have been carried out at a temperature of 30 °C, whereas it was 50 °C for the AL study.[34] These temperatures were chosen to ensure that the lipids simulated, DMPC and DPPC, respectively, were in the (biologically relevant) liquid-crystalline phase. Moreover, in the AL simulations[34] the bilayer interfacial area was artificially kept fixed to avoid known artifacts of the particular AL force-field employed,[75] whereas in the AL−CG study we have implemented the (more realistic) semi-isotropic pressure coupling, which allows the *xy* interfacial plane to fluctuate according to the lateral components of the pressure tensor. Finally, there are differences in the way diffusion coefficients were computed. The integral involved in the calculation of $D_z(z)$ (reported in the Supporting Information) is typically characterized by slowly converging tails, which can undermine the reliability of the estimation of the diffusion coefficient. To avoid such problems, the integral is sometimes fitted to an analytical function;[34,68,69] however, when sufficiently long simulations are performed, no fitting is required.[62,63] In the AL study by Bemporad et al.,[34] the force fluctuation autocorrelation function had to be approximated by fitting to analytical functions because of the limited simulation time (10 ns per solute's *z*-location). The AL−CG runs were instead sufficiently long (80 ns) to yield converged values without resorting to approximations.

In both the AL[34] and the AL−CG models, it is difficult to clearly identify how the limitations and artifacts, inherent in each of the models, affect the results. The general tendency would be to consider the AL data more accurate. However, we have already noted that experimental data[53] on the free energy difference between the headgroup region and the water phase for acetic acid indicate a value $\Delta G \approx -0.45$ kJ/mol. This finding is inconsistent with the AL results of Bemporad et al., which yielded a positive free energy difference.[34] Also, a number of experiments have shown that short-chain alcohols, and in particular methanol, preferentially partition inside the bilayer, corresponding to the headgroup-glycerol region.[54−58] Considering the free energy curves from permeability simulations, those experimental observations[54−58] are consistent with our multiscale results and incompatible with the AL data of Bemporad et al.,[34] that predict a partitioning location for methanol in the water phase, outside the membrane. Also, other more recent AL simulation studies[59−61] support the predictions of our multiscale AL−CG model that methanol and acetamide preferentially partition inside the membrane, approximately at the lipid headgroup−tail interface.

A general note must be made regarding the investigation of the transmembrane permeability of water. The inhomogeneous solubility−diffusion mechanism,[5−7] which is at the basis of our calculation, is accepted by many as the dominant mechanism for the passive permeation of solutes across biomembranes.[76] For water and ionic solutes however, another mechanism, based on transient water pores, has been proposed.[77] So far, experiments have not provided decisive evidence. Simulations have the potential to shed light on the issue, although very large length and time scales might be required, as it is estimated that the formation of only one pore requires two thousand lipids.[77]

An important aspect of our multiresolution approach concerns its transferability to different systems. We have recently conducted permeability simulations of large molecules such as β-blocker drugs and steroid hormones,[73] employing essentially the same protocol presented here; in particular, we used the same values for the multiscale parameters α and β. Partitioning locations and relative permeability coefficients proved in agreement with atomistic simulation data and experimental measurements.[73] While further work is needed to properly assess the transferability and generality of our method, these results are very encouraging.

Conclusion

We have presented a new multiresolution methodology based on the direct compatibility between our recently developed coarse-grain (CG) membrane model[25] and a standard atomic-level (AL) force-field. The method has been applied to simulate the transmembrane permeation process of small AL solutes embedded in a hydrated CG lipid bilayer. Permeability calculations have been carried out by applying a new *z*-constraint algorithm which properly conserves total momentum and force. The permeability properties calculated by multiscale simulation compare favorably with previous computational investigations and available experimental data. Importantly, the permeability ranking order between the solutes is accurately predicted. Overall, the multiscale AL−CG methodology presented allows

simulations to benefit from an efficiency speed-up of 2 orders of magnitude over traditional AL methods, while retaining generality and accuracy.

Acknowledgment. This work has been funded by Johnson & Johnson and the Biotechnology and Biological Sciences Research Council (BBSRC).

Supporting Information Available: Summary of experimental studies, the *z*-constraint method, full velocity-Verlet algorithm including our reformulated *z*-constraint scheme, coarse-grain force-field parameters, and inertial features of permeant molecules. This material is available free of charge via the Internet at http://pubs.acs.org.

References and Notes

(1) Pohorille, A.; Wilson, M. A. *Cell. Mol. Biol. Lett.* **2001**, *6*, 369–374.
(2) Xiang, T.-X.; Anderson, B. D. *Adv. Drug Delivery Rev.* **2006**, *58*, 1357–1378.
(3) Overton, E. *Vierteljahrsschr. Naturforsch. Ges. Zuerich* **1896**, *41*, 383.
(4) Finkelstein, A. *J. Gen. Physiol.* **1976**, *68*, 127–135.
(5) Diamond, J. M.; Katz, Y. *J. Membr. Biol.* **1974**, *17*, 121–154.
(6) Diamond, J. M.; Szabo, G.; Katz, Y. *J. Membr. Biol.* **1974**, *17*, 148–152.
(7) Marrink, S.-J.; Berendsen, H. J. C. *J. Phys. Chem.* **1994**, *98*, 4155–4168.
(8) MacCallum, J. L.; Tieleman, D. P. In *Computational Modeling of Membrane Bilayers*; Feller, S. E., Ed.; Elsevier, New York, 2008; Chapter *8*, pp 227−256.
(9) Orsi, M.; Essex, J. W. In Molecular Simulations and Biomembranes: From Biophysics to Function; Biggin, P. C., Sansom, M. S., Eds.; Royal Society of Chemistry: in press.
(10) Muller, M.; Katsov, K.; Schick, M. *Phys. Rep.* **2006**, *434*, 113–176.
(11) Brannigan, G.; Lin, L. C. L.; Brown, F. L. H. *Eur. Biophys. J.* **2006**, *35*, 104–124.
(12) Orsi, M.; Sanderson, W.; Essex, J. W. In *Molecular Interactions—Bringing Chemistry to Life*; Hicks, M. G., Kettner, C., Eds.; Beilstein-Institut: Germany, 2007; pages 185−205. (Also available online at http://www.beilstein-institut.de/bozen2006/proceedings/Orsi/Orsi.pdf.)
(13) Xiang, T.-X.; Anderson, B. D. *J. Membr. Biol.* **1994**, *140*, 111–122.
(14) Ayton, G. S.; Noid, W. G.; Voth, G. A. *Curr. Opin. Struct. Biol.* **2007**, *17*, 192–198.
(15) Woods, C. J.; Mulholland, A. J. In *Chemical Modelling: Applications and Theory*; Hinchliffe, A., Ed.; Royal Society of Chemistry: Cambridge, U.K., 2008.
(16) Sherwood, P.; Brooks, B. R.; Sansom, M. S. P. *Curr. Opin. Struct. Biol.* **2008**, *18*, 630–640.
(17) Abrams, C. F. *J. Chem. Phys.* **2005**, *123*, 234101.
(18) Neri, M.; Anselmi, C.; Cascella, M.; Maritan, A.; Carloni, P. *Phys. Rev. Lett.* **2005**, *95*, 218102.
(19) Neri, M.; Anselmi, C.; Carnevale, V.; Vargiu, A. V.; Carloni, P. *J. Phys.: Condens. Matter* **2006**, *18*, S347−S355.
(20) Shi, Q.; Izvekov, S.; Voth, G. A. *J. Phys. Chem. B* **2006**, *110*, 15045–15048.
(21) Ensing, B.; Nielsen, S. O.; Moore, P. B.; Klein, M. L.; Parrinello, M. *J. Chem. Theory Comput.* **2007**, *3*, 1100–1105.
(22) Praprotnik, M.; Delle Site, L.; Kremer, K. *Phys. Rev. E* **2006**, *73*, 066701.
(23) Praprotnik, M.; Delle Site, L.; Kremer, K. *J. Chem. Phys.* **2007**, *126*, 134902.
(24) Praprotnik, M.; Matysiak, S.; Delle Site, L.; Kremer, K.; Clementi, C. *J. Phys.: Condens. Matter* **2007**, *19*, 292201.
(25) Orsi, M.; Haubertin, D. Y.; Sanderson, W. E.; Essex, J. W. *J. Phys. Chem. B* **2008**, *112*, 802–815.
(26) Michel, J.; Orsi, M.; Essex, J. W. *J. Phys. Chem. B* **2008**, *112*, 657–660.
(27) Gay, J. G.; Berne, B. J. *J. Chem. Phys.* **1981**, *74*, 3316–3319.
(28) Liu, Y.; Ichiye, T. *J. Phys. Chem.* **1996**, *100*, 2723–2730.
(29) Fennell, C. J.; Gezelter, J. D. *J. Chem. Phys.* **2004**, *120*, 9175–9184.
(30) Chandra, A.; Ichiye, T. *J. Chem. Phys.* **1999**, *111*, 2701–2709.
(31) Jorgensen, W. L.; Chandrasekhar, J.; Madura, J. D.; Impey, R. W.; Klein, M. L. *J. Chem. Phys.* **1983**, *79*, 926–935.
(32) Berendsen, H. J. C.; Grigera, J. R.; Straatsma, T. P. *J. Phys. Chem.* **1987**, *91*, 6269–6271.
(33) Tan, M.-L.; Brooks, B. R.; Ichiye, T. *Chem. Phys. Lett.* **2006**, *421*, 166–170.
(34) Bemporad, D.; Essex, J. W.; Luttmann, C. *J. Phys. Chem. B* **2004**, *108*, 4875–4884.
(35) Schaftenaar, G.; Noordik, J. H. *J. Comput.-Aided Mol. Des.* **2000**, *14*, 123–134.
(36) *AMBER 8 User's Manual*; University of California: San Francisco, CA, 2004.
(37) Wang, J. M.; Wolf, R. M.; Caldwell, J. W.; Kollman, P. A.; Case, D. A. *J. Comput. Chem.* **2004**, *25*, 1157–1174.
(38) Jakalian, A.; Bush, B. L.; Jack, D. B. *J. Comput. Chem.* **2000**, *21*, 132–146.
(39) Xiang, T.-X.; Chen, X. L.; Anderson, B. D. *Biophys. J.* **1992**, *63*, 78–88.
(40) Feenstra, K. A.; Hess, B.; Berendsen, H. J. C. *J. Comput. Chem.* **1999**, *20*, 786–798.
(41) Allen, M. P.; Tildesley, D. J. *Computer Simulation of Liquids*, 1st ed.; Oxford Science Publications: Oxford, U.K., 1987.
(42) Cleaver, D. J.; Care, C. M.; Allen, M. P.; Neal, M. P. *Phys. Rev. E* **1996**, *54*, 559–567.
(43) Golubkov, P. A.; Ren, P. *J. Chem. Phys.* **2006**, *125*, 064103.
(44) Price, S. L.; Stone, A. J.; Alderton, M. *Mol. Phys.* **1984**, *52*, 987–1001.
(45) Marrink, S.-J.; Berendsen, H. J. C. *J. Phys. Chem.* **1996**, *100*, 16729–16738.
(46) Roux, B.; Karplus, M. *Biophys. J.* **1991**, *59*, 961–981.
(47) Roux, B.; Karplus, M. *J. Phys. Chem.* **1991**, *95*, 4856–4868.
(48) BRAHMS: A Biomembrane Reduced-Approach Molecular Simulator, http://www.personal.soton.ac.uk/orsi/brahms/ (accessed July 28, 2009).
(49) Dullweber, A.; Leimkuhler, B.; McLachlan, R. *J. Chem. Phys.* **1997**, *107*, 5840–5851.
(50) Berendsen, H. J. C.; Postma, J. P. M.; van Gunsteren, W. F.; Di Nola, A.; Haak, J. R. *J. Chem. Phys.* **1984**, *81*, 3684–3690.
(51) The Iridis Compute Cluster, http://www.southampton.ac.uk/isolutions/computing/hpc/iridis/ (accessed July 28, 2009).
(52) Nagle, J. F.; Tristram-Nagle, S. *Biochim. Biophys. Acta* **2000**, *1469*, 159–195.
(53) Xiang, T.-X.; Anderson, B. D. *J. Membr. Biol.* **1995**, *148*, 157–167.
(54) Chiou, J.-S.; Krishna, P. R.; Kamaya, H.; Ueda, I. *Biochim. Biophys. Acta* **1992**, *1110*, 225–233.
(55) Rottenberg, H. *Biochemistry* **1992**, *31*, 9473–9481.
(56) Barry, J. A.; Gawrisch, K. *Biochemistry* **1994**, *33*, 8082–8088.
(57) Holte, L. L.; Gawrisch, K. *Biochemistry* **1997**, *36*, 4669–4674.
(58) Feller, S. E.; Brown, C. A.; Nizza, D. T.; Gawrisch, K. *Biophys. J.* **2002**, *82*, 1396–1404.
(59) Patra, M.; Salonen, E.; Terama, E.; Vattulainen, I.; Faller, R.; Lee, B. W.; Holopainen, J.; Karttunen, M. *Biophys. J.* **2006**, *90*, 1121–1135.
(60) MacCallum, J. L.; Bennett, W. F. D.; Tieleman, D. P. *Biophys. J.* **2008**, *94*, 3393–3404.
(61) Johansson, A. C. V.; Lindahl, E. *J. Chem. Phys.* **2009**, *130*, 185101.
(62) Shinoda, W.; Mikami, M.; Baba, T.; Hato, M. *J. Phys. Chem. B* **2004**, *108*, 9346–9356.
(63) Sugii, T.; Takagi, S.; Matsumoto, Y. *J. Chem. Phys.* **2005**, *123*, 184714.
(64) Jedlovszky, P.; Mezei, M. *J. Am. Chem. Soc.* **2000**, *122*, 5125–5131.
(65) Bassolino-Klimas, D.; Alper, H. E.; Stouch, T. R. *Biochemistry* **1993**, *32*, 12624–12637.
(66) Bemporad, D.; Luttmann, C.; Essex, J. W. *Biochim. Biophys. Acta* **2005**, *1718*, 1–21.
(67) Grossfield, A.; Woolf, T. B. *Langmuir* **2002**, *18*, 198–210.
(68) Ulander, J.; Haymet, A. D. J. *Biophys. J.* **2003**, *85*, 3475–3484.
(69) dos Santos, D. J. V. A.; Eriksson, L. A. *Biophys. J.* **2006**, *91*, 2464–2474.
(70) Walter, A.; Gutknecht, J. *J. Membr. Biol.* **1986**, *90*, 207–217.
(71) Alper, H. E.; Stouch, T. R. *J. Phys. Chem.* **1995**, *99*, 5724–5731.
(72) Vaz, W. L. C.; Almeida, P. F. *Biophys. J.* **1991**, *60*, 1553–1554.
(73) Orsi, M.; Sanderson, W. E.; Essex, J. W. submitted for publication.
(74) Feller, S. E.; Mackerell, A. D. *J. Phys. Chem. B* **2000**, *104*, 7510–7515.
(75) Sonne, J.; Jensen, M. Ø.; Hansen, F. Y.; Hemmingsen, L.; Peters, G. H. *Biophys. J.* **2007**, *92*, 4157–4167.
(76) Paula, S.; Volkov, A. G.; Vanhoek, A. N.; Haines, T. H.; Deamer, D. W. *Biophys. J.* **1996**, *70*, 339–348.
(77) Jansen, M.; Blume, A. *Biophys. J.* **1995**, *68*, 997–1008.
(78) Lande, M. B.; Donovan, J. M.; Zeidel, M. L. *J. Gen. Physiol.* **1995**, *106*, 67–84.
(79) Orbach, E.; Finkelstein, A. *J. Gen. Physiol.* **1980**, *75*, 427–436.
(80) Hill, W. G.; Rivers, R. L.; Zeidel, M. L. *J. Gen. Physiol.* **1999**, *114*, 405–414.

(81) Walter, A.; Gutknecht, J. *J. Membr. Biol.* **1984**, *77*, 255–264.
(82) Bar-On, Z.; Degani, H. *Biochim. Biophys. Acta* **1985**, *813*, 207–212.
(83) Nagle, J. F.; Mathai, J. C.; Zeidel, M. L.; Tristram-Nagle, S. *J. Gen. Physiol.* **2008**, *131*, 77–85.
(84) Bloom, M.; Evans, E.; Mouritsen, O. G. *Q. Rev. Biophys.* **1991**, *24*, 293–397.
(85) Carruthers, A.; Melchior, D. L. *Biochemistry* **1983**, *22*, 5797–5807.
(86) Cevc, G.; Marsh, D. *Phospholipid Bilayers—Physical Principles and Models*, 1st ed.; John Wiley & Sons: New York, 1987.
(87) Humphrey, W.; Dalke, A.; Schulten, K. *J. Mol. Graphics* **1996**, *14*, 33–38.

JP903248S